CERN-PPE-97-092

EUROPEAN LABORATORY FOR PARTICLE PHYSICS

CERN-PPE/97-092
15th July 1997

The extended OPAL silicon strip microvertex detector

S. Anderson [d], J. R. Batley [a], G. A. Beck [c], T. Behnke [b], M. Bobinski [c], A. A. Carter [e], J. R. Carter [a], S. J. de Jong [d], U. C. Dunwoody [a], V. Gibson [a], W. Glessing [b], M. J. Goodrick [a], E. Gross [i], R. Hammarström [b], G. G. Hanson [d], M. Hapke [c], A. K. Honma [h,1], F. Jacob [f], M. Jiminez [b], C. R. Jones [a], P. Jovanovic [g], T. Junk [b], P. Kyberd [e], J. A. Lauber [b,2], A. J. Martin [e], A. McNab [e], R. Mir [i], K. Mühlemann [b], T. W. Pritchard [e], D. R. Rust [d], R. Van Kooten [d]

[a] *Cavendish Laboratory, Cambridge, CB3 0HE, UK*
[b] *CERN, European Organisation for Particle Physics, 1211 Geneva 23, Switzerland*
[c] *Fakultät für Physik, Albert Ludwigs Universität, D-79104 Freiburg, Germany*
[d] *Indiana University, Dept. of Physics, Swain Hall West 117, Bloomington, Indiana 47405, USA*
[e] *Dept. of Physics, Queen Mary and Westfield College, University of London, London, E1 4NS, UK*
[f] *Rutherford Appleton Laboratory, Chilton, Didcot, Oxfordshire, OX11 0QX, UK*
[g] *School of Physics and Space Research, University of Birmingham, Birmingham B15 2TT, UK*
[h] *University of Victoria, Dept. of Physics, P. O. Box 3055, Victoria, BC, V8W 3P6, Canada*
[i] *Weizmann Institute of Science, Particle Physics Dept., P. O. Box 26, Rehovot, Israel*

Abstract

The OPAL experiment at the CERN LEP collider recently increased the geometrical acceptance of its silicon microvertex detector. The azimuthal coverage is improved by adding one pair of detector modules to each of the two layers, while the polar angle coverage is extended by adding new detector modules in line with the existing ones. This improves the efficiency for high quality tracking in OPAL and in particular for b quark tagging in Higgs boson searches. A description of the detector is given, with emphasis on new or modified elements with respect to the earlier version. Results on the performance of the new detector are presented.

Submitted to Nuclear Instruments and Methods A

[1] Also at TRIUMF, Vancouver, BC, V6T 2A3, Canada
[2] Present address: Dept. of Physics, University College, London WC1E 6BT, UK

1 Introduction

OPAL is one of four large general purpose experiments operating at the LEP e^+e^- collider at CERN [1]. The experiment achieves excellent charged particle tracking and momentum measurements using the combined properties of a silicon strip microvertex detector, a vertex drift chamber, a large acceptance high resolution jet-type drift chamber, and chambers specialised in measurement of the z coordinate[†], all contained in a solenoidal magnetic field of 0.435 T. Outside the tracking detectors are segmented electromagnetic and hadronic calorimeters for energy measurements of particles and jets. The outermost detection layer of the experiment consists of streamer tubes and drift chambers for muon identification. The addition of the silicon microvertex detector to OPAL became possible after the first LEP run in 1989 when it was found that the low beam backgrounds permitted the use of a smaller diameter beam pipe. The desire for a high spatial resolution strip detector was primarily motivated by the need to measure or identify particles with typical decay lengths at LEP of several millimeters (such as b flavoured hadrons and τ leptons) and to search for new particles having similar decay lengths. The first OPAL silicon strip microvertex detector (μVTX1) [2] was installed and began data taking in June 1991. It consisted of two concentric layers of single-sided silicon detector wafers with AC coupled readout strips at 50 μm pitch oriented for azimuthal (ϕ) coordinate measurement. The original proposal for a microvertex detector for OPAL envisaged a two-coordinate readout device, the single coordinate μVTX1 being an interim step until the techniques for two-coordinate readout were perfected. The two coordinate version of the OPAL silicon strip microvertex detector (μVTX2) was installed and began operation in June 1993 [3].

The excellent single hit resolutions of μVTX1 and μVTX2 were demonstrated in Z^0 di-lepton decays, where the impact parameter resolutions were measured to be $\sigma(d_0) = 15$ μm in the plane perpendicular to the beam direction and, for μVTX2 where the orthogonal coordinate was also measured, $\sigma(z_0) = 20$–50 μm in the direction along the beam, for polar angles ranging from $|\cos\theta| = 0$ to 0.8, respectively. The use of the μVTX1 and μVTX2 information resulted in a significant improvement in tracking for OPAL, which has been demonstrated in precision measurements for the τ lepton [4] and b flavoured hadron lifetimes [5], as well as in the identification of b quark events [6]. The addition of a precise measurement of the z coordinate in tracking near the vertex with the μVTX2 has allowed three-dimensional vertex reconstruction and has reduced the number of tracks falsely associated with the reconstructed vertex. The result is improved signal over background for exclusive b flavoured hadron reconstruction and b flavour tagging.

In autumn 1995, the LEP collider entered a new era in which the centre-of-mass energy is being raised in steps from the Z^0 resonance to about 200 GeV. One of the main goals of this LEP2 phase of operation is the search for the Higgs boson. In the Standard Model the Higgs boson decays dominantly into $b\bar{b}$ quark pairs (85% branching ratio). The same is true for large parts of the parameter space of the Minimal Supersymmetric Standard Model, the simplest supersymmetric extension of the Standard Model [7]. To distinguish Higgs bosons from the irreducible background due to Z^0 and $W^\pm$ decays, b quark tagging is indispensable and the highest possible tagging efficiency and purity should be attained. In view of this new physics to be explored at the LEP collider, the OPAL silicon strip microvertex detector was upgraded to provide the largest possible geometrical acceptance (μVTX3). The position of the μVTX3 inside

[†]The OPAL coordinate system is defined with the z-axis in the positron beam direction, y in the upward direction and x towards the center of the LEP ring. The azimuthal angle ϕ is the angle with respect to the x axis in the x–y plane, and the polar angle θ is the angle with respect to the z axis.

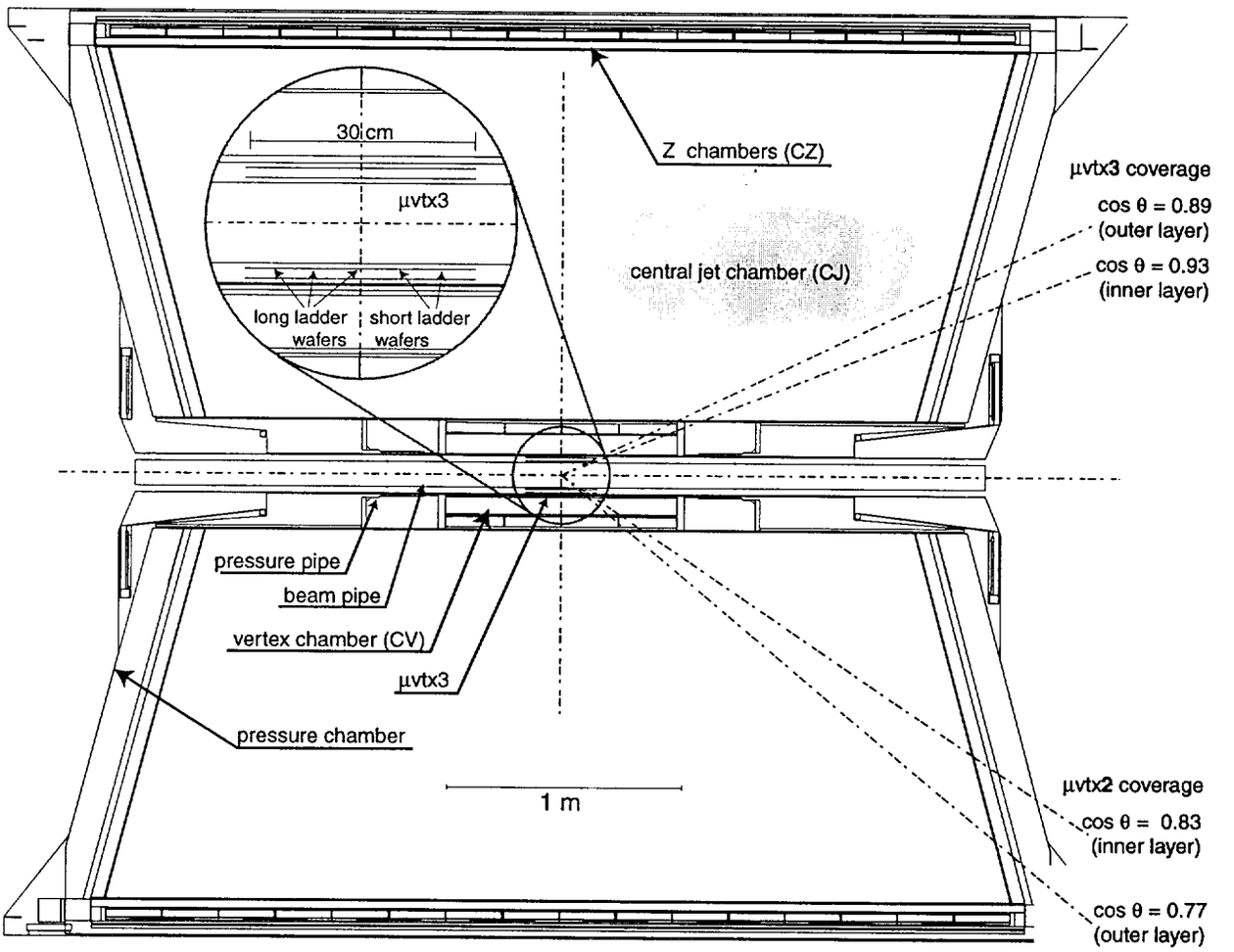

Figure 1: *The OPAL silicon microvertex detector μVTX3, shown within the overall tracking system. The centre of the drawing has been enlarged in an eyeglass view. The extent of the μVTX3 silicon wafers, i.e. the active detection area, has been indicated by a line for each layer. The dash-dotted lines indicate the fiducial coverage in the polar angle (θ–coordinate), for the inner and outer barrel respectively, in the upper right quadrant for the present μVTX3 detector and in the lower right quadrant for the previous version of the detector (μVTX2).*

the OPAL tracking system is shown in Fig. 1. In the same figure, the geometrical acceptance in the polar coordinate is indicated. The acceptance in the polar coordinate has increased from $|\cos\theta| < 0.77$ for the μVTX2 to $|\cos\theta| < 0.89$ for μVTX3 for two-layer coverage. The azimuthal angle coverage has improved from 80% for μVTX2 to 97% for μVTX3 for two-layer coverage.

The radiation monitoring system for the μVTX3 was also substantially improved. This system now also allows for a fast beam dump in the event of very high radiation doses occurring in very short times. The new radiation monitoring system is described in a separate paper [8].

In the next section a brief overview of the entire system will be given. As a large part of the μVTX3 detector is similar to that of μVTX2, this paper will concentrate on the modifications and new features in the μVTX3 detector. In the following sections the mechanical design, the front-end electronics, the data acquisition and online processing, the powering, cooling and monitoring system and the offline processing are described, and a performance overview is then given.

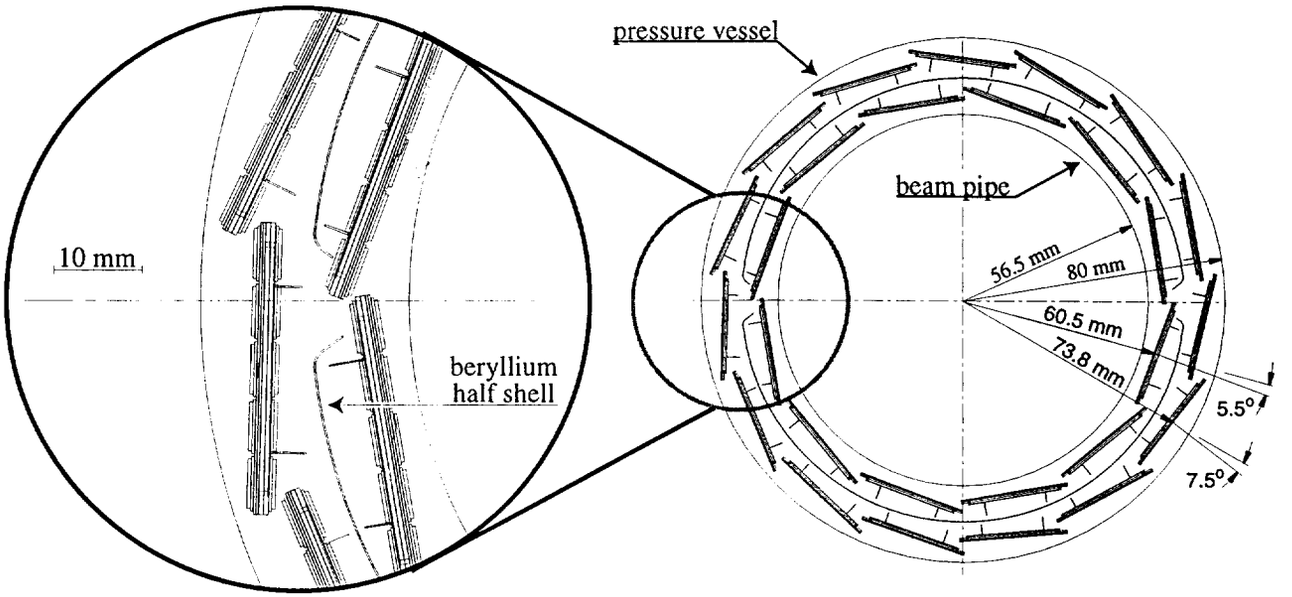

Figure 2: *End-on view of the geometrical ladder configuration. The important radial dimensions are indicated. On the left, part of the figure is magnified, showing more details of the structure and illustrating the tight mechanical tolerances.*

2 Overview of the extended OPAL silicon strip microvertex detector

The OPAL silicon strip microvertex detector is constrained to fit in an annular space between the beam pipe, with a maximum outer diameter of 56.5 mm, and the wire chamber pressure vessel, with an inner diameter of 80 mm (see Fig. 2).

The μVTX2 consisted of 25 *ladders* arranged in two concentric layers around the beam pipe, 11 ladders on the inner cylindrical detection layer and 14 ladders on the outer layer. A ladder consisted of three pairs of back-to-back ϕ and z wafers aligned end-to-end.

For the μVTX3 the geometrical coverage is increased in two ways. The coverage in ϕ is made almost complete by adding one more ladder to each cylindrical detection layer. This brings the number of ladders in the inner layer to 12 and in the outer to 15. To extend the coverage along the z direction, 27 new ladders are added. The μVTX2 ladders are reused after structural modification and are called *long ladders*. This distinguishes them from the newly added *short ladders*, which are of similar construction but shorter in length, consisting of two pairs of ϕ and z wafers each. Long ladders and short ladders are aligned longitudinally with their readout electronics on opposite ends of the detector. Figure 3 shows such a long and short ladder pair. Figure 4 shows how these ladder pairs are arranged to form the μVTX3 OPAL silicon microvertex detector.

The shorter length of the new ladders was determined by a constraint on the overall length of the microvertex detector. This is due to the limited length of the beam pipe that can be accessed for the assembly of the microvertex detector. The choice was made to install the detector around the beam pipe in two half shells (as was done for the μVTX1 and μVTX2) and to have the entire length of long and short ladders preassembled before installation. Splitting the detector in the z direction in two or more pieces was not practical, given the precision with which the sensitive parts of the detector have to be aligned.

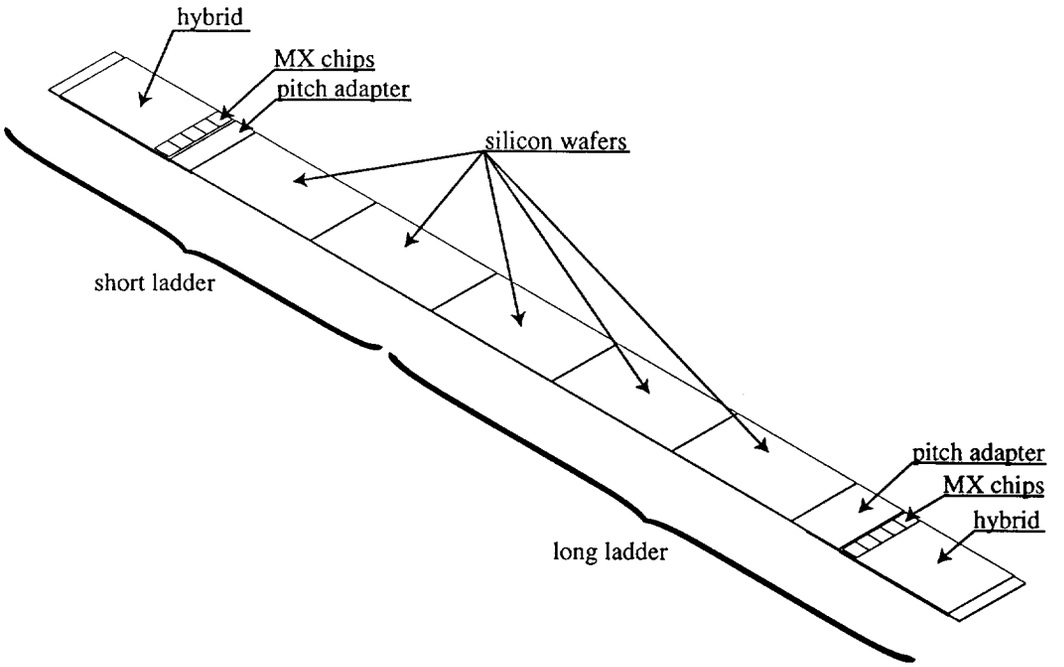

Figure 3: *Simplified schematic of an OPAL μVTX3 long and short ladder pair. The ϕ readout side is facing upwards.*

In azimuthal coverage the ladders are arranged with a small tilt angle with respect to the circumference so that the detectors have a small overlap, as shown in Fig. 2. The available radial space does not allow an overlap in sensitive detector area, but the dead region between the ladders in the ϕ coordinate has become negligible.

For both short and long ladders, the ends with readout electronics are mounted on two support rings, one of which contains a cooling tube. The other ends, which meet close to the centre of the OPAL detector, are supported from structures that are glued onto the beryllium support half-shells. These shells link the support rings at the two ends and provide mechanical stability to the complete assembly.

The ladder electronics are connected via short cables to seven InterConnect Ring cards (ICR cards) on each side of the detector. These ICR cards hold additional transceiver and amplifier electronics and provide the interconnections to the cables that lead to the outside of the OPAL detector through the annular space between the beam pipe and the wire chamber pressure vessel. In contrast to the μVTX2, cables are routed out on both sides of the OPAL detector, rendering the installation procedure significantly more complex.

Just outside the OPAL magnet return yoke the cables connect to patch panels from where larger diameter cables are routed to the counting room, which houses all the data acquisition, powering and control electronics. The existing cabling of the μVTX2 is used on one side of OPAL and on the other side similar cabling and patch panels have been added. The necessary equipment in the counting room has been doubled to cope with the doubling of the number of ladders.

The μVTX3 ladders are cooled with temperature regulated water that is circulated through cooling tubes in the support rings. A new cooling system has been added to that existing for the μVTX2, to give independent cooling for the long and the short ladder sides.

Some key parameters of the μVTX3 detector are listed in Table 1.

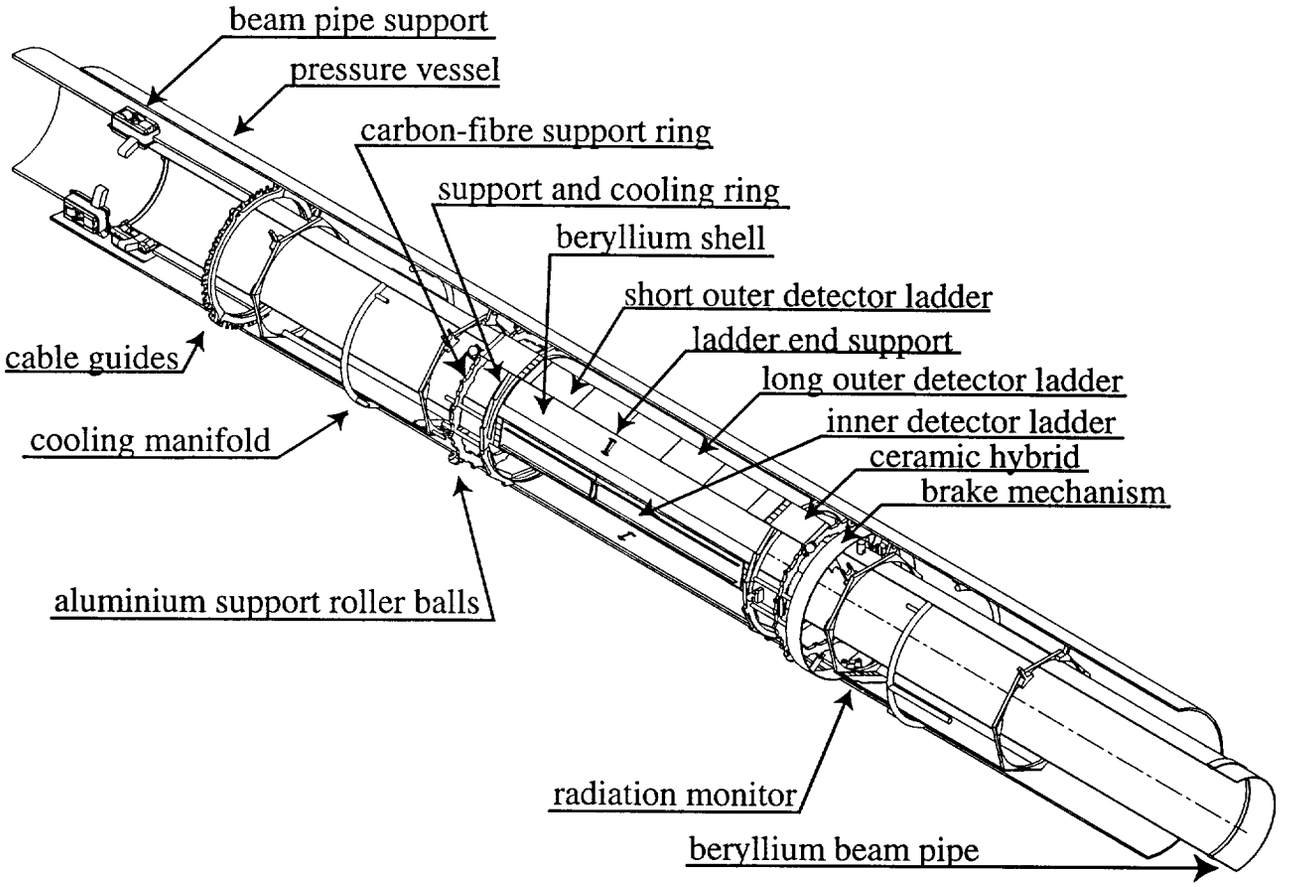

Figure 4: *Cut-away view of the μVTX3 OPAL silicon microvertex detector.*

μVTX3 parameter	Value
Number of ladders per layer	12 (inner), 15 (outer)
Effective radius of layer	60.5 mm (inner), 73.8 mm (outer)
maximum $\lvert\cos\theta\rvert$ acceptance	0.93 (inner), 0.89 (outer)
ϕ acceptance	97.8% (inner), 99.6% (outer)
Average material thickness	1.5% X_0 at normal incidence
Strip biasing method	FoxFET (gated reach-through channel)
2 coordinate detection	back-to-back ϕ and z single-sided detectors
z readout scheme	aluminium or gold printed circuit on 200 μm thick glass
Number of active channels	65 502
Readout chip, noise, power	MX7, 350e+15e/pF, 2 mW/channel
	MX7-RH, 320e+21e/pF, 2 mW/channel
Signal-to-noise ratio	24 (ϕ) and 20 (z) (long ladders),
	29 (ϕ) and 25 (z) (short ladders)
Radiation hardness	$\sim$500 Gy (MX7 chip)
Cooling method	water cooling
Fraction of good channels	$\approx$99%

Table 1: *Characteristics of the μVTX3 OPAL microvertex detector.*

3 Mechanical design

3.1 The support structure

The overall system assembly is shown in Fig. 4. The ladders are assembled onto a supporting structure consisting of two polygonal aluminium alloy rings joined by a 0.2 mm thick shell of beryllium. These parts are epoxy bonded using a cold setting compound [9]. The points on the support rings to which the ladders are fixed are provisionally aligned by traversing the structure under a microscope table using as reference the 1.5 mm diameter dowel pin holes which are later used to align the ladders themselves. The beryllium shells [10] were supplied primed for the epoxy bonding process, and no further operations were made on them during assembly. The shells are shaped as half cylinders, but with the long edges bent inwards for extra rigidity. In the first set of shells that were delivered some cracks were found in the region where the beryllium was bent inwards. This problem was of metallurgical nature and was not present in a second iteration.

The aluminium alloy rings provide good thermal contact to the hybrids carrying the front-end electronics. The cooling is provided through a stainless steel manifold fitted to a semicircular groove machined in the ring. The manifold and the aluminium alloy ring were indium plated before being soldered together with indium (melting point 156°C) and a resin flux. The flux was carefully removed using hot water and solvents immediately after the assembly. The manifold was fitted before final machining to minimise distortions of the final structure resulting from differing coefficients of thermal expansion of the components. Final machining to generate the surfaces that are used to align the ladders was made by the electro-erosion process, which is both very precise and exerts a minimum of pressure on the part. The surface area for thermal contact was of necessity small, and further reduced by fixing hardware. The tapped holes were therefore not chamfered and the surfaces were carefully lapped to present a maximum flat area to the hybrid.

The outer ends of the ladders are supported by a machined carbon-fibre ring with aluminium alloy thread inserts glued with epoxy [11]. The whole structure rolls into position on hollow aluminium alloy spheres rolling on the inner surface of the wire chamber pressure vessel. These rolling spheres are fixed to the outer rings of the detector (see Fig. 4) and provide the basic support for the detector structure.

The coolant circuit was made from stainless steel and polyurethane plastic tubes, and was pressure tested during installation up to 4 bar above atmospheric pressure. A slight underpressure is maintained at the detector during normal operation, and the water pressure is limited to 2.5 bar at the detector with an overpressure valve located at the pump.

3.2 Ladder end support

In the μVTX2, the ladder ends away from the electronics were fixed to support rings by flat aluminium plates that were part of the ladder support frames. For the μVTX3, the ladder ends of the long and short ladders meet near the centre of the OPAL detector, where there must be both minimal material and minimal dead space between the active detector wafers. This is achieved by removing the aluminium fixing plate that was part of the μVTX2 ladder design and instead supporting these ladder ends from the beryllium shells with the structures shown in Fig. 5. These structures consist of two hollow beryllium pins held by a carbon-fibre/polymethacrylimide-foam/carbon-fibre sandwich glued onto the beryllium shells. The ladders have a carbon-fibre support piece glued onto the extremity of their z-prints and stiffener

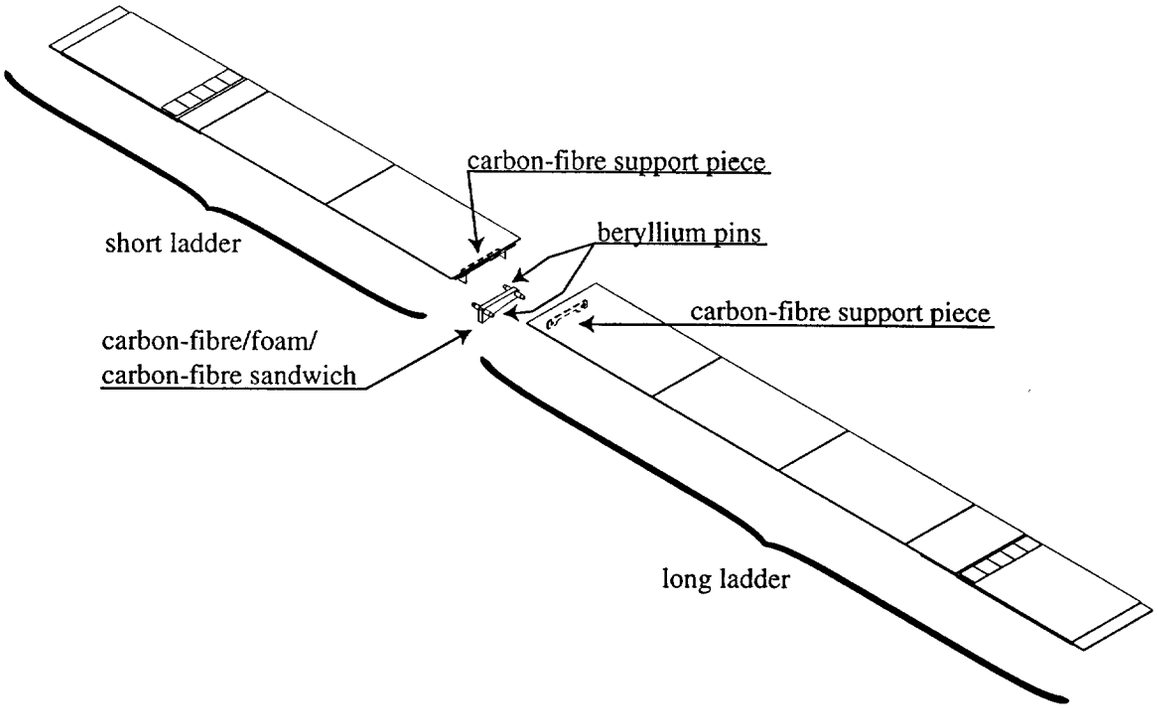

Figure 5: *Detail of the end support pieces glued onto the beryllium shells to support the ladder ends.*

ribs, with one round and one slotted hole that engage the two beryllium pins, as described in the next section.

3.3 Short ladder structure

The short ladders are similar in construction to the long ladders, but the design has been modified in a number of ways to suit the needs of the μVTX3 and to profit from the experience gained in the construction of the long ladders.

The components needed to construct a short ladder are shown in an exploded schematic drawing in Fig. 6. There are two ϕ and two z FoxFET detector wafers [12] of dimension 60×33 mm^2 and 250 μm thickness, an aluminium printed circuit on 200 μm thick glass for z readout ("z-print"), an aluminium print on quartz to adapt the readout pitch of the ϕ detector to that of the amplifier chips ("pitch adapter"), two thick film hybrid printed circuit boards ("hybrids"), one for each readout side, made on beryllia (BeO) substrates which carry the readout chips and surface-mounted electronic components, two kevlar/epoxy stiffener ribs, an aluminium support plate with a fibre-glass/epoxy skeleton frame glued to it, the frame serving as a spacer between the z-print and back-to-back detector wafer sandwich, and finally a carbon-fibre support piece glued to the z-print and between the stiffener ribs at the ladder end. This locating plate is part of the new ladder end fixing scheme described in the previous section.

The z-print [13] has essentially the same layout as for the long ladders, but is shorter by the 60 mm length of one detector wafer. The long ladder z-prints used for the μVTX2 had gold print on glass. For the μVTX3, an aluminium print on glass was chosen as this gives better properties for bonding and removes a problem of occasional shorts resulting from the chromium adhesion layer that was used under the gold print. The new masks for the z-print fabrication

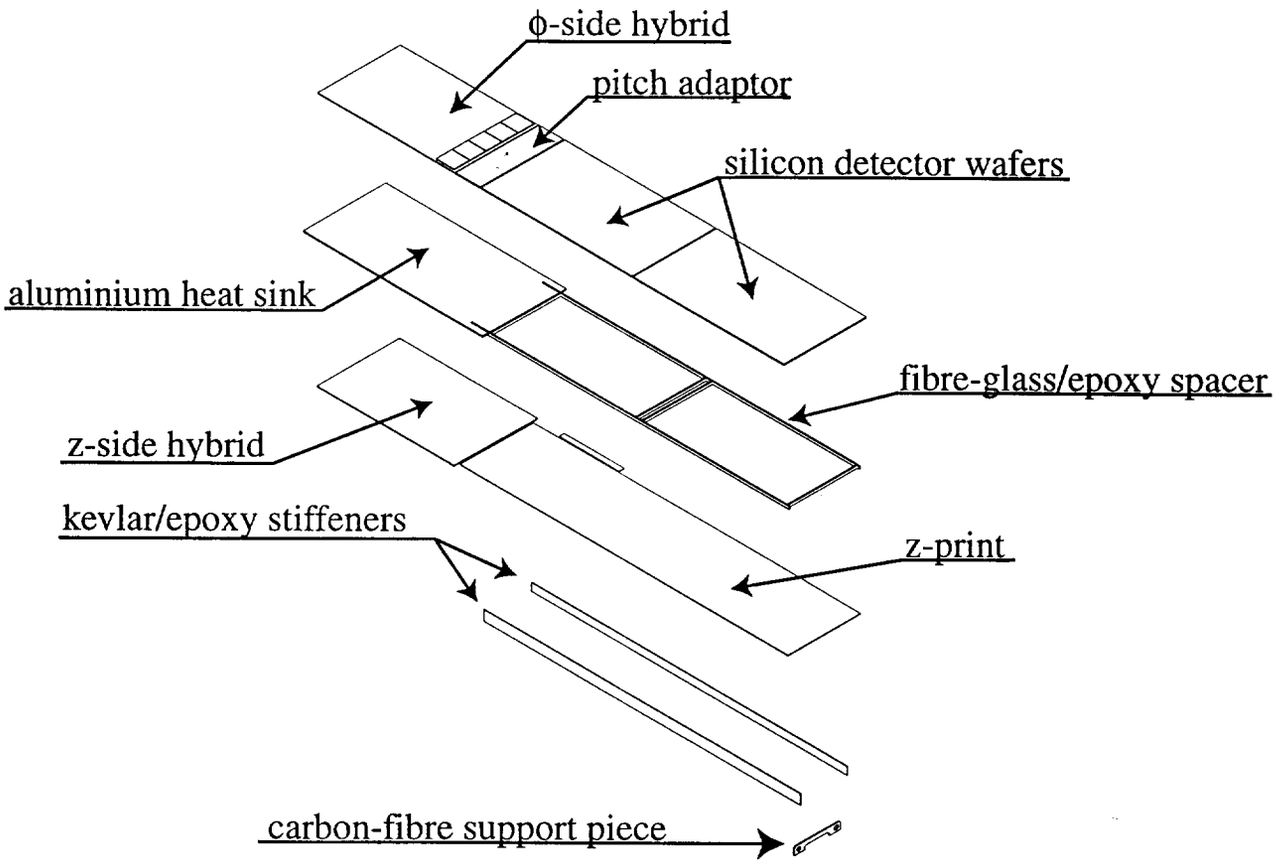

Figure 6: *Schematic exploded view of a short μVTX3 ladder.*

took account of the different etching properties of aluminium compared with gold on glass, and clear line numbering was included to assist in diagnosing problems and repairs. As in the construction of μVTX2, all delivered prints were inspected for shorts or breaks in the traces, but the process was speeded up by using a specialised semi-automatic optical apparatus to test for line discontinuities and a custom made probe card to measure shorts between adjacent lines [14]. To improve the visibility of problems, the z-prints were positioned on a mirror, such that the print was illuminated both from the front and from the back. The back of the print could be brought into focus under a microscope via the mirror to distinguish between real open circuits and dirt spots or superficial scratches on the surface.

Small numbers of shorts or opens found in the inspection were repaired where possible by bonding across breaks or cutting away shorts. The resulting z-prints used in construction had less than 0.3% line faults. The quartz pitch adapters were also inspected for shorts and opens, and repaired to a similar standard.

To minimise the length of μVTX3, the pitch adapters used in the new ladders are 14 mm shorter than those of the long ladders. The two stiffener ribs are now also of different height. This is because, in the new tilted ladder geometry, one of the ribs lies closer to the beryllium shell than in μVTX2, and the original rib height cannot be accommodated.

The ladder assembly is very similar to that of the long ladders and has been described in detail in [3].

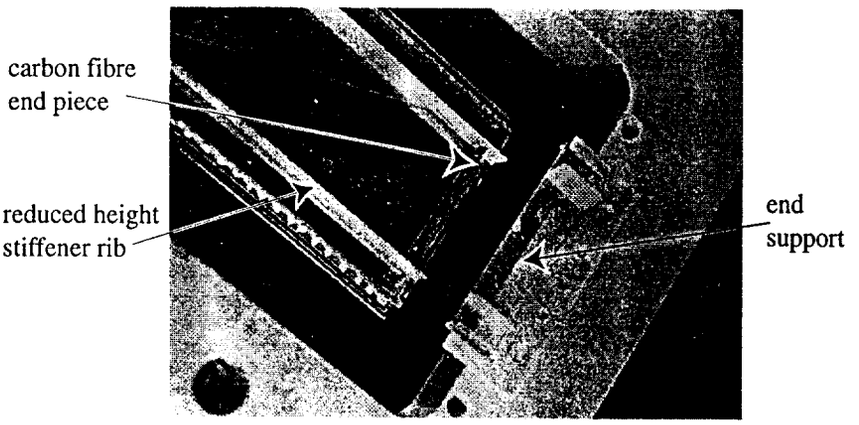

Figure 7: *Modified long ladder carried over from the μVTX2. The end support piece cut off by the diamond wire saw is shown on the right. The difference in height between the two stiffener ribs can also be seen.*

3.4 Long ladder modifications

Two structural changes had to be made to all the long ladders to make them suitable for the μVTX3 geometry: the aluminium plate at the end of each ladder was cut off, and the height of one of the two kevlar/epoxy stiffener ribs was reduced. Both operations were extremely delicate, as they were performed on completed ladders, and were achieved after careful development of appropriate tooling and procedures.

To reduce its height, one rib was cut in one pass by a CO_2 laser, holding the ladder enclosed in a box fixture with the rib projecting through a narrow slot. The box was pressurised with dry nitrogen to reduce as far as possible any smoke or debris resulting from the cut reaching the sensitive area of the detector. Despite these precautions, a significant amount of burnt, carbonised, kevlar/epoxy debris reached the z-prints, causing some shorts between lines. After these particles had been carefully cleaned off, the full functionality of all ladders was restored.

To remove the end piece of the long ladders, a cut had to be made through the glass z-print, the fibre-glass/epoxy frame, and the kevlar/epoxy stiffener ribs. The cut was made as close as possible to the end of the silicon detector wafers. The process adopted was to use a saw made from a wire encrusted with fine diamond powder. The saw [15] uses approximately 10 metres of 300 μm diameter wire encrusted with 30 μm diamond powder. The saw mechanism allows the wire to be off-wound, passed through the cutting zone, and rewound onto the same bobbin. The winding direction is then reversed and the process repeated until the cut is completed. The cut was made using distilled water as the coolant and lubricating medium, and for swarf removal. The holding fixture was designed as a closed box so that the detector could be maintained under dry gas overpressure by a supply of nitrogen. The detector ladder was placed in the fixture with the cut zone corresponding to a 2 mm wide slot in the fixture. To further reduce the ingress of water towards the silicon wafers a pair of thin copper shim curtains were fitted close to the cutting area. The pressurised gas leaking past these curtains tended to keep the wafers dry. The end of the detector was held by a suction pad adjacent to the cutting area so that the unsupported (cantilevered) structure was stabilised at this point when the sawing wire broke through the detector ladder structure. Despite the effort to keep debris and cooling water away from the ladders, they still received significant amounts of these from cutting, but no damage resulted from this process. Some difficulties were encountered from small cracks produced in some z-prints in the corner where the sawing wire broke through, and some damage

was incurred due to the necessarily complicated handling needed to set up the sawing process. However, no ladder was lost due to the sawing procedure, and at most one or two channels on a ladder were affected by these difficulties.

Figure 7 shows a photograph of a long ladder used in the μVTX2 system with the end support piece cut off. In the same picture the difference in height can be observed between the two stiffener ribs.

The cutting away of the end fixing plate necessitated the addition of the new carbon-fibre support piece designed to receive the two precision locating pins, described in the previous section. Again, this was glued to the z-print and between the stiffening ribs, as for the short ladders.

The modifications described provided the only means of reusing the original detectors and were made on a very tight time schedule between the removal of the original array at the start of the shut-down period and reinstallation of the lengthened array at the end of the same shut-down (about 4 months).

3.5 Ladder testing, repairs and results

Procedures similar to those used for μVTX2 were adopted to test and repair the new short ladders of μVTX3. These are described in detail in reference [3]. All detector wafers were subjected to visual inspection and long-term leakage current tests before use (their individual channels having already been probe-tested by the manufacturer). The hybrid readout and the wafer leakage currents were re-tested at critical points in the ladder assembly process.

After completion of the ladder, all possible repairs due to, for example, bonding faults or z-print damage, were carried out on the individual channels. As will be discussed in section 5, it was also necessary to replace a small number of MX7-RH amplifier chips on the hybrids that had failed during construction.

The completed ladders were subjected to thorough tests to verify the quality of the readout, the expected depletion voltage, the signal-to-noise measured with a ^{106}Ru β source, and the long-term stability of both the leakage currents and the readout quality.

A total of 48 short ladders were made, of which 32 were of the highest quality for the experiment, with more than 99% good channels in both ϕ and z and completely stable ladder leakage currents of less than 1 μA. A further 9 ladders provide additional acceptable spares for the detector, all with excellent leakage current performance and more than 98% good channels. A further 4 ladders also have more than 95% good channels, and only 3 ladders were of an unusably poor quality due to problems in their construction or bonding.

4 Metrology

The precise knowledge of the position and orientation of the silicon wafers with respect to each other was for the μVTX2 mostly acquired by a software alignment procedure using Z^0 decay data. Although the ultimate alignment information still relies on such a procedure (see section 8), the production rate of tracks needed for software alignment is greatly reduced for collecting data at energies above the Z^0 peak. Nevertheless, a fast detector calibration is desirable for rapid analysis of new data at high energies. For these reasons a careful optical survey of the μVTX3 was made prior to its installation, to ensure a reasonably accurate starting point for the software alignment procedure.

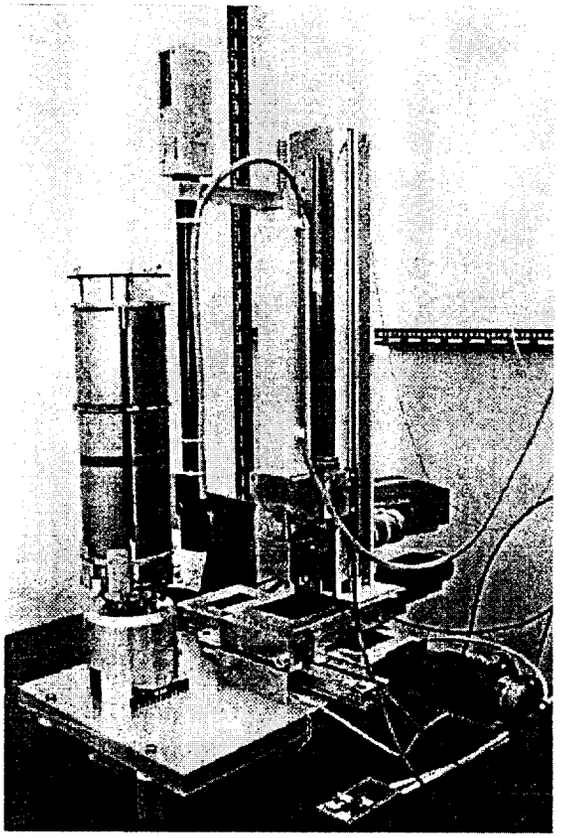

Figure 8: *Photograph of the dedicated optical measuring apparatus, with the μVTX3 beryllium support shells mounted on the left.*

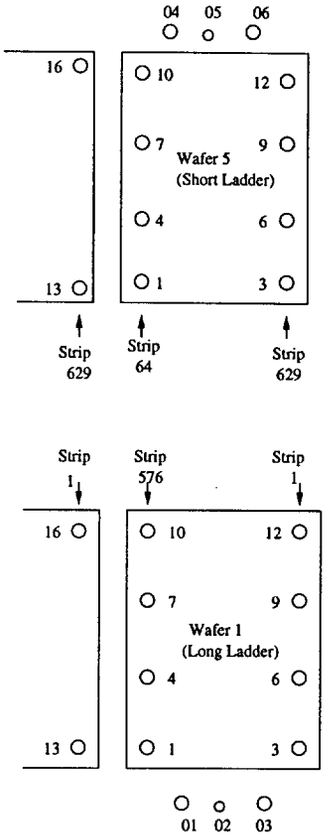

Figure 9: *Schematic of survey points for each silicon wafer.*

4.1 Measurements of ϕ face coordinates of the ladders and the support structure

Metrology on the detector array was performed on a dedicated apparatus (see Fig. 8) consisting of a four-axis coordinate table. To optimise safe operation, table movements were motorised with a high reduction gearing and movements were all under manual control only. The coordinate positions were measured on linear ($3\times$) and rotary ($1\times$) scales [16] read out by digital displays [17]. The intrinsic accuracy of this system is ± 5 μm for the linear and rotary scales. The digital display readings were logged directly through the interface to a MVME147 CPU [18] running the OS9 [19] operating system, placed in a VME crate.

The dedicated measuring apparatus was verified and calibrated using an aluminium tube machined to have flat surfaces similar to those on the real structure. This tube was first precisely measured by the CERN metrology service and then measured again with the apparatus to calibrate its distance scales.

The point to be measured was viewed by a CCD camera on the vertical axis and a periscope style lens system having a focal length of 45 mm. This allowed the internal elements of the μVTX3 to be viewed with minimum risk since the measuring head remained at a safe distance away from the detector. To accurately measure the radial position, which is along the viewing

axis, the measured point was illuminated by a simple laser diode pointer at 45° to the lens viewing axis. The pointer was modified by fitting a converging lens in the light beam, focusing it at approximately 25 mm and positioned to correspond to the camera lens focal point. Thus a pin-point of red light was visible on the object to be measured. The monitor was fitted with a digitally generated cross-hair fiducial. The measuring process was therefore to place the fiducial in the image on a given feature on the wafer, then to bring the laser point to the fiducial by varying the distance from the camera to the surface, and then to log the position, with the actual focusing of the camera image not being critical.

The points that were measured for each wafer are depicted in Fig. 9. The three-dimensional position of these points was measured with the ladders mounted on the support structure. The complete set of measurements (27×56) was taken in about 24 hours.

To translate the measured points into starting positions for the software alignment procedure there are two concerns. The first is that the detector structure has been measured with the z coordinate pointing up in the earth's gravitational field, while in OPAL the z coordinate is in the horizontal plane. Thus mechanical deflections due to gravitational forces may be different. The second, more significant, point where discrepancies may arise comes when the structure is partly disassembled from a full cylinder into two half cylinders needed for installation, resulting in shifts of one half cylinder with respect to the other. For the operation of splitting into two half cylinders, eight ladders (four long and four short) have to be removed to be mounted again during the detector installation. For these eight ladders the information from the metrology measurements represents less accurately their actual positions after installation.

By repeating measurements, the metrology procedure itself was found to be reproducible to about 5 μm. Splitting the full assembly into two half cylinders and joining them again was observed to give a shift in the relative z positions of the two half cylinders of about 100 μm, while the relative alignments within the half cylinders were also affected at the 100 μm level.

The measurement along the z–axis with the metrology apparatus gave significantly poorer results than the r–ϕ measurements. Therefore the information on the z alignment was taken from measurements described in the next section.

4.2 Measurements of the z face coordinates of the ladders

The optical measurements of the assembled structure described in the previous section could only be made on the r–ϕ faces of the ladders. The z faces of the ladders in both the inner and outer detector layers lie towards the beryllium support shell (Fig. 2) and so are optically inaccessible. The positions of the z face silicon wafers on each ladder relative to the r–ϕ wafers were therefore measured in a separate process before the ladder was assembled on the structure. This information was then used to provide the position and orientation of the z wafers of each ladder on the assembled detector, given the direct measurement of the assembled r–ϕ ladder wafer positions as described above.

Two separate measurements were made on each ladder to establish the coordinates of the z face wafers with respect to those of the r–ϕ face, using x–y moving stages under manual control. Firstly, the planar coordinates of the wafers on each side of the ladder were measured, referenced to the same precision ladder mounting points, i.e. the dowel in the hybrid and supports at the ladder end (section 4.1). Four reference points were measured at the corners of each wafer to a precision of about 5 μm. The second measurement required was the separation between the r–ϕ and z wafers across the thickness of a ladder. This distance was measured directly at both edges of every ladder, at 20 mm intervals along its length, to a precision of about 10 μm.

4.3 Installation in OPAL and overall system assembly

The overall system assembly is shown in Fig. 4. The detector itself is in the middle of the structure and has an overall length of 458 mm, including both the long and short ladders with their front-end electronics. On both ends of the detector there are InterConnect Rings (ICR) with their own cooling manifolds. They contain seven printed circuit boards (PCBs), each connected to the detector with short cables and miniature connectors. The ICR PCBs contain transceiver electronics and a sequencer chip that controls the serial readout of ladder pairs. At the end away from the detector, cables are soldered onto the ICR cards.

From the ICR cards the cables are supported for the length of the pressure pipe by five cable wagons of total length 1.7 m on each side. These cable wagons rest on the pressure pipe via the plastic cooling tubes.

On one side of the detector a braking ring mechanism allows the μVTX3 to be firmly located relative to the pressure pipe within OPAL. The braking mechanism consists of an expanding ring that can be pushed outwards, remotely controlled by stainless steel wires passed out along the pressure pipe with the cables. One of these wires is also used to gauge the distance of the detector from the end of the pressure pipe, and hence control the positioning of the detector in the z-coordinate with respect to the central wire chambers.

On the long ladder side the detector is directly coupled to the cable wagons. The detector is moved by pushing or pulling the cable wagons on the long ladder side. On the short ladder end there is a free space of 58 mm between the detector and the first cable wagon. This distance is measured and maintained when the detector is pushed into position by moving the cable wagons on the short ladder side. The cable wagons on both sides are moved simultaneously so that minimal forces are exerted on the detector structure.

The μVTX2 had output cables from one end only. The beam pipe vacuum chamber had a central support ring which was located near to the detector at the end where there were no cables. The μVTX3 has cables from both ends which makes it incompatible with this central vacuum chamber support. A new support is therefore now incorporated into the cable wagon system for μVTX3. Near the detector the vacuum chamber is supported from a set of jacks whose positions can be adjusted by means of a stainless steel cable, thereby regulating the pressure exerted on the beam pipe in four directions. In addition, there are freely accessible supports for the vacuum chamber at both ends of the OPAL detector.

For LEP2 operation at high beam energies, additional shielding of the experiment against synchrotron radiation is necessary. For this purpose, a tungsten mask has been mounted inside the vacuum chamber at each end of the experiment, complemented by a thick shield located just outside the vacuum pipe. The latter have been incorporated in place of a cable wagon by making the outermost unit on each side from a cylinder of tungsten alloy 5 mm thick, 130 mm diameter and 300 mm long. This heavy tungsten alloy cable wagon is supported by acetal rollers from the pressure pipe. Lead cylinders are also placed around the beam pipe in the space between the end of the pressure pipe and the tungsten alloy cable wagon for additional shielding.

At installation, the detector is fitted around the beam pipe in two halves. To have sufficient access to make the connection of the two half barrels, a total of eight ladders (two pairs on each side) had to be assembled after the fitting around the beam pipe, using a special jig. This jig holds the ladders in a vacuum chuck that can be carefully manipulated in all axes to allow the ladders to slide under the already mounted neighbour in the overlap region. The procedure is illustrated in Fig. 10. During this operation the detector array can be rotated around the vacuum tube such that the ladder fitting platform is always in the same position.

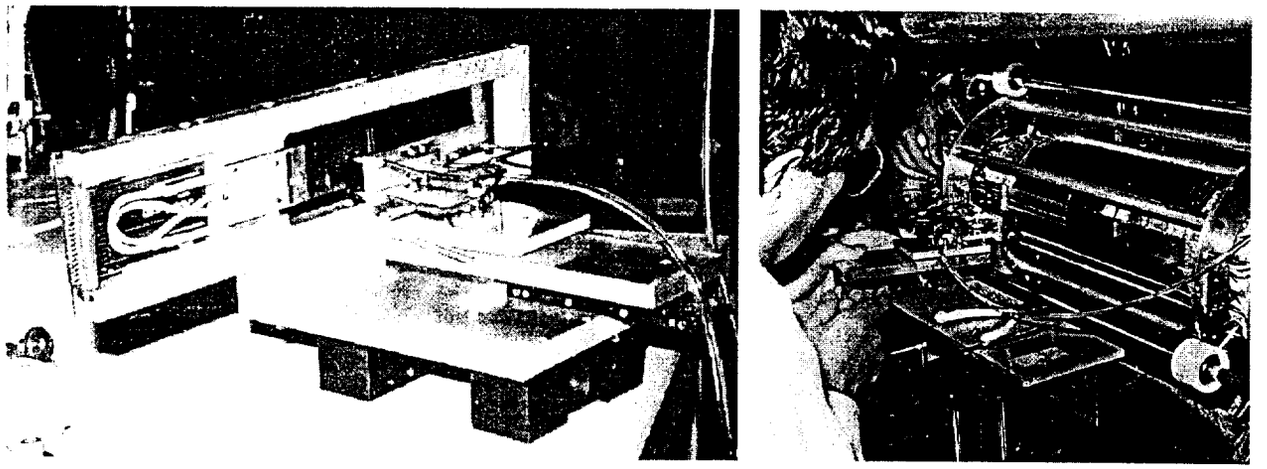

Figure 10: *Photographs showing the picking up and installation of one of the last eight ladders.*

The detector installation is complicated by the fact that cables come out at both ends of the pressure vessel. The vacuum chamber is temporarily supported from its end flanges on a sliding rig, allowing it to be offset and therefore increase the length available for assembly. In the installation procedure, one ICR and its associated cable wagons are first pushed completely through the pressure pipe from one side of the OPAL experiment to the other. The detector is then fitted around the beam pipe and connected to this ICR. The detector is next moved into the pressure pipe and the other ICR is fitted and connected. The detector is then moved to the centre of OPAL and cable wagons are added at the side that is pushed in. Finally, the vacuum chamber is brought into its definitive position and the support jacks are activated.

Initially a major problem was caused by the frictional forces to be overcome as the cables were pushed completely through the pressure pipe with the first ICR and cable wagon assembly. This was overcome by very carefully tying the cables on temporary supports.

After the installation was complete the volume between the vacuum chamber and the pressure pipe was carefully sealed at the ends. Dry nitrogen is blown into this volume at a rate of 150 litres per hour through a plastic tube that ends near the detector. Gas samples are continuously extracted and checked for humidity and oxygen content.

5 Front-end electronics

5.1 Overview

The silicon detector strips from each side of a ladder are connected to the front-end electronics located on hybrids at the end of the ladder. The front-end electronics consists of five MX7 Microplex readout chips and a local sequencer control chip [3]. The local sequencers are in turn controlled via the ICR card logic by a FASTBUS Master Sequencer module, which is located in a counting room outside of the OPAL detector. Each MX7 Microplex chip receives the detector signals from 128 strips and stores the associated charge for each channel on every beam crossing. After an event trigger the 128 signal charges are read out sequentially as analogue signals. The analogue signals are received by line drivers situated on the ICR cards which transmit the signals outside the OPAL detector to FASTBUS SIROCCO IV [20] modules which digitise, store and process the data (see section 6.3). The local sequencers and MX7 chips allow test calibration pulses to be injected into the front-end amplifiers of each readout channel. In

addition the common wafer backplane bias line can be pulsed to check the functioning of the complete readout chain.

5.2 The MX7 microplex readout chips

5.2.1 Evolution of the MX7 chips

The new short ladders of μVTX3, with two wafers per module side, are equipped with radiation hard MX7 VLSI readout chips (MX7-RH), fabricated in the Harris 1.2 μm AVLSI-RA process [21]. These chips have been developed by the Rutherford Appleton Laboratory microelectronics group from the successful MX7 version, previously fabricated in the 1.5 μm Mietec CMOS process, and which are used for reading out the long ladders of μVTX3 [22].

The decision to develop a more radiation tolerant version of the MX7 chip arose because Mietec chips from different processing runs have variable levels of radiation tolerance, down to values approaching those that might be experienced during the expected lifetime of LEP running. After irradiation, the signal risetime from Mietec MX7 chips increases. Tests made in the laboratory using a 10 mCi ^{90}Sr source have shown that running the chips in the normal high power mode, with the bandwidth limit on, results in the risetime increasing from about 0.4 μs before irradiation to about 4 μs after 700 Gy. This risetime is to be compared with the integration time of 1.8 μs in the experiment. The performance of the chip after significant irradiation can largely be recovered by running with the bandwidth limit off, where the risetime is about 1.4 μs after 700 Gy. The Master Sequencer (section 6.2) has been modified for μVTX3 to allow the bandwidth limit control to be set individually for each hybrid on each ladder in case of high levels of radiation in OPAL. It is expected that the signal-to-noise performance of the more radiation tolerant of the Mietec chips can be maintained at better than 80% of the initial value up to 700 Gy. The corresponding figure for the least tolerant batches of chips is about 300 Gy.

As a consequence of this, the long ladders that have the more radiation tolerant Mietec chips have been placed in the inner of the two detector layers, nearest the beams, where the background radiation is highest. The maximum integrated dose on a ladder at the end of the 1996 data-taking period was 14 Gy [8], and so far no deterioration due to radiation has been observed for any of the long ladders.

However, it was decided to use new radiation-hard MX7-RH chips for the construction of the short ladders for the extended detector, thus providing additional contingency against the effects of the increased synchrotron radiation expected at the higher LEP2 energies.

5.2.2 Design features of MX7-RH chips

The MX7-RH chips maintain the basic architecture of the original MX7 version, but are detailed to new fabrication rules, and have a smaller die area. The layout is optimised to provide minimum degradation in pulse risetime by removing radiation-dependent sensitivity to the charge integration circuitry.

The new chip is $\sim$375 μm thick and has an area of 36 mm^2 with mixed analogue and digital functions, providing 128 low noise amplifiers, filters and an analogue output multiplexer. Each microvertex ladder side is read out by five chips with daisy-chained control and readout bus-lines. Each channel consists of a charge amplifier and bandwidth filter, with the output connected by switches to two storage capacitors. The low frequency noise sensitivity is minimised by operating these in a double-correlated sample-and-hold mode as for the Mietec version. The

MX7-RH is run in high power mode, dissipating 2.1 mW per channel. The post-filter signal has a risetime of 400 ns and is integrated for about 1.8 μs. With these conditions the noise performance of the chip, as a function of input load capacitance, is 320 + 21/pF (rms) electrons.

Samples of MX7-RH chips have been subjected to extensive gamma irradiation studies using ^{60}Co sources, and shown to operate successfully even after doses of up to 1 MGy. With such intrinsic tolerance to radiation no degradation of performance is expected over the lifetime of operation of these devices at LEP, and none has so far been seen.

5.2.3 Testing the MX7-RH chips

Each Harris wafer was probed before being diced, to establish which chips had all channels functioning and were thus considered candidates for further tests. Although there were significant variations in device yield between different wafers, some wafers did achieve values as high as 65%. After dicing, the candidate chips were each subjected to detailed tests, with the recorded information stored in a data-base. A 25-pin custom-designed probe card was used to contact individual chips, and measurements were made for all 128 channels of: raw pedestals, mean noise per channel, pulse heights from calibration inputs, effective gain versus channel number, cross-talk from adjacent channels in calibration mode, and linearity of response to calibration input. The complete measurement sequence was carried out twice on each chip to ensure reproducibility of results.

The result of these detailed tests after dicing was to reject about a further 15% of the chips. The selection process provided a very valuable quality control element as well as establishing tight limits on amplifier gain and response risetime specifications for each chip. The majority of chips came from a single processing batch and showed gain variations at the 10% level within and between wafers. However, two other processing batches were less satisfactory, with variations up to 40%, and these chips were matched in gain in sets of 5 to populate a given hybrid. The performance of the chips from these two batches was also inferior, resulting in a 20% reduction in signal-to-noise on the ladder.

During chip testing and ladder assembly very careful handling of the MX7-RH chips was necessary to avoid chip mortality through electrostatic discharge, but even so about 2% of good chips were lost for this reason. However, only one chip from more than 500 that have been assembled into ladder readout hybrids has so far shown any failure after being commissioned within a working ladder.

5.3 Modified hybrids for MX7-RH and the new InterConnect Ring circuit boards

The electronic hybrids for the MX7-RH used for the short ladders are very similar to those used on the long ladders [3]. The changes involve adaptation to the different (smaller) physical dimension of the microplex chip and adjustment of components for setting the optimal working voltage of the MX7-RH.

Since seven additional ICR circuit boards were needed for μVTX3, it was decided to replace all cards on both sides of the detector. This provided the opportunity to improve the layout and suppress complications arising from unused supplementary circuitry on the μVTX2 ICR cards. In addition the layout of the drain and guard bias voltage wiring was changed to allow better measurement of leakage currents.

6 Data acquisition and online processing

6.1 Overview

The general layout of the data acquisition system is shown in Fig. 11. It is an improved version of the system used for the μVTX2 [3] based on an OPAL VME Local System Crate (LSC) [23], interfaced to two FASTBUS crates that are now needed for the independent readout of each side of the detector.

The LSC controls the local readout system and links the microvertex detector to the global OPAL trigger [24] and readout system [23]. Each FASTBUS crate is connected via a FASTBUS VSB Interface (FVSBI) [25] to a FIC processor [26] in the LSC, which controls the readout of each FASTBUS crate independently. Once the data are stored in VME memory they are handed to the master processor, a MVME167 [27], which merges the event and handles the connection to the global OPAL readout. In this way the readout time is nearly the same as for the μVTX2 system, even though twice the amount of data is now read out. Each FASTBUS crate is devoted to the readout of one side of the microvertex detector directed by a custom built FASTBUS control and timing module, the Master Sequencer. The data are digitised, processed and buffered in 14 SIROCCO IV modules [20] per crate. Online processing of the data performed by the digital signal processors (DSPs) [28] on the SIROCCO modules includes pedestal subtraction and cluster finding which results in a large data reduction factor.

6.2 Upgrade of the Master Sequencer

The new Master Sequencer (MSEQ3) follows the same principles as those used in μVTX1 and μVTX2. This FASTBUS module is the central steering device of the readout system. It is connected to a VME clock-module, which is synchronised by the LEP accelerator cavity radio frequency, and it provides the overall timing and control signals needed for the front-end electronics and the digitising electronics in the SIROCCO modules. Of the eight control output channels, seven are connected to local sequencers on the ladders, and one is a spare. In the Master Sequencer version for the μVTX2 (MSEQ2) these outputs could be separately enabled or disabled by writing an 8-bit word to a register. By subsequently loading a new sequence into the Master Sequencer and writing to this register it was possible to drive each local sequencer differently if needed. The time and storage overhead at the beginning of a run would have been acceptable. However, operation of the μVTX1 detector already suggested that the flags set in the local sequencers at the beginning of a run were sometimes corrupted by the readout operation, and so it became practice to add a global flag setting sequence at the end of every readout sequence. The time and storage overhead for addressing every local sequencer with a different flag sequence after every readout would not have been negligible. As there are now two different kinds of MX7 chips in operation, with the possibility of radiation damage in the LEP2 environment of the Mietec MX7 chips, the need to use this feature could well arise. To solve this problem the RAM width was increased from 8 to 16 bits, the extra 8 bits driving the output-enable register of the MSEQ3. This allows the different local sequencers to be individually addressed from within one sequence. Even assuming the worst case that all local sequencers need different settings, the time penalty would now be only 100 μs.

An incident in the 1995 running period required the implementation of another new feature. The signal to start the sample-and-hold cycle is derived from the beam crossing signal by a NIM module. This module failed in such a way that it randomly suppressed the output of the signal, whose arrival was not checked on an event-by-event basis in the Master Sequencer. The

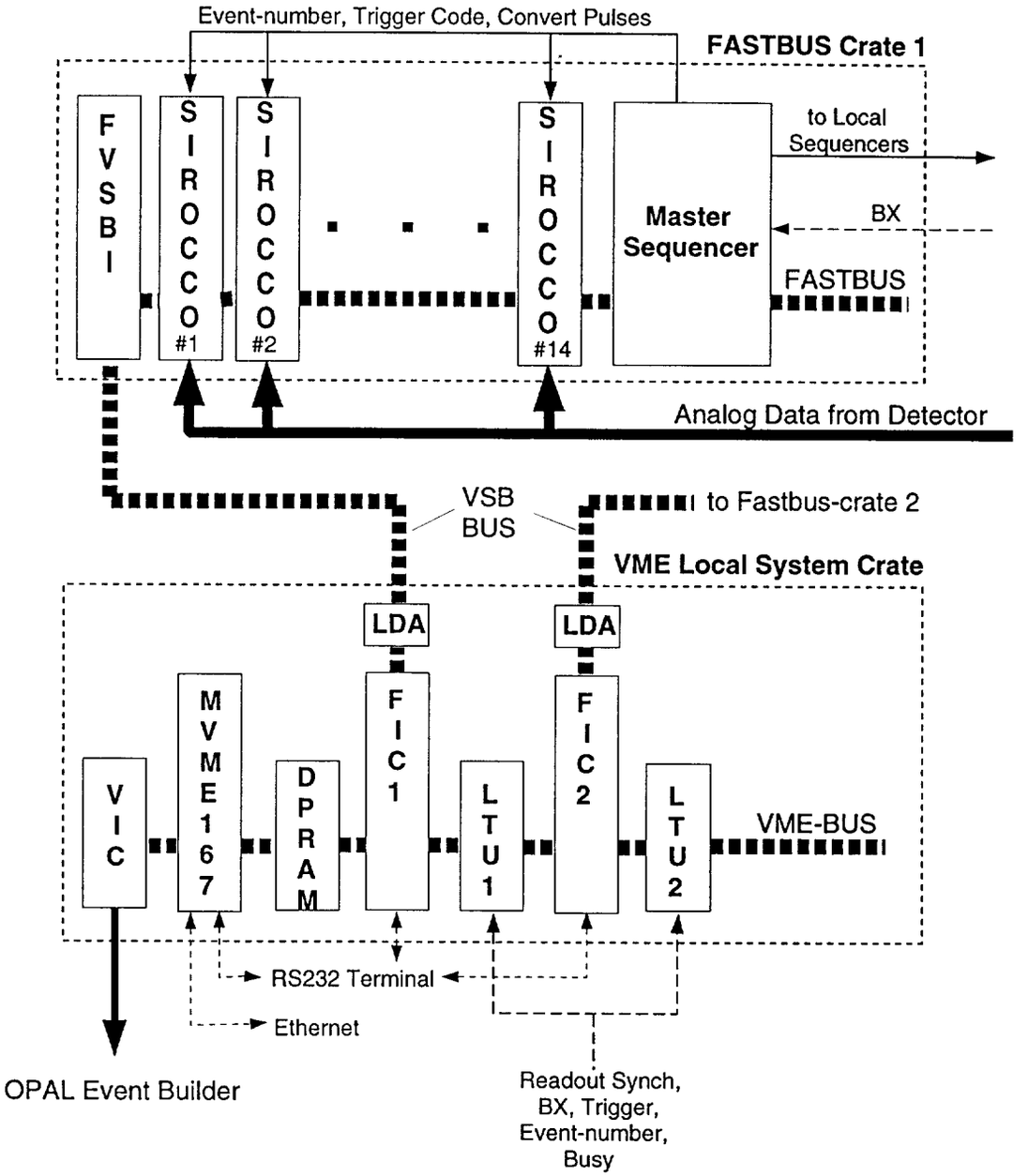

Glossary of Terms

SIROCCO: FADC + 2x DSP56001 (22MHz)	VIC: VME Interconnect Module
FVSBI: Fastbus to VSB Interface	DPRAM: Dual Ported RAM
LDA: Long Distance Adapter	LTU: Local Trigger Unit
FIC(8230): MC68020 Processor (16MHz)	MVME167: MC68040 Processor (25MHz)

Figure 11: *General layout of the μVTX3 data acquisition system.*

following trigger signal then led to the readout of an old event from the front-end hold-and-keep buffer. To protect against such failures, a flag in the Master Sequencer is now set by the incoming beam crossing signal and cleared by either a reset signal in the absence of a trigger, or by the end of readout following a trigger. The flag is read out and checked before starting the readout to make sure that a new event has been recorded in the front-end.

6.3 Online data processing

Except for some improvements described below, the online processing is the same as for μVTX2 [3]. For LEP2 operation the ratio of background events and real e^+e^- interactions has dramatically increased compared with the LEP1 data at the Z^0 peak. High occupancy background events, in which many of the channels of an MX7 chip are active, appear to the online system as pedestal shifts. To avoid this behaviour, the DSP and FIC software have been changed to update pedestal and noise values only on certain low occupancy triggers. An unused bit in one of the trigger words that are sent from the FIC to the DSPs is set or cleared to steer whether or not the pedestal and noise values are to be updated. For the 1996 LEP2 running, pedestal and noise updates were done only in the absence of a track trigger, which corresponded to approximately 40% of all triggers.

7 Powering, cooling and monitoring

7.1 Overview

The powering, cooling and detector environmental monitoring systems for the previous version of the detector [3] have been duplicated for running the two sides of μVTX3.

The control of the systems is based on a single VME crate (separate from that of the data acquisition system) containing a processor [27], several interface modules, and a 32 channel VME ADC [29] module with several multiplex modules attached to its inputs. The control hardware runs on battery backed-up non-interruptable power supplies [30]. The powering system, completely replaced since the previous version of the OPAL microvertex detector and described in section 7.2, is no longer on a non-interruptable supply. The VME crate now also houses a temperature interlock system module, described in section 7.3.

The two independent cooling systems are controlled via VME interface modules by the above mentioned VME CPU. A temperature regulation system has been implemented in software to stabilise the temperature at the detector wafers to the level of 0.1°C (rms).

Power control, cooling control, and monitoring software communicate with the global OPAL Slow Controls system [31]. This allows control actions to be centralised and error messages to be entered into the error message utility [32] system and displayed on appropriate screens in the OPAL control room and elsewhere. A memory register in the VME cooling module and a separate dedicated memory register VME module are both connected to a hardware system that can generate warning and alarm messages on a dedicated screen in the OPAL control room. The processor indicates changes of detector status (for example, whether the detector is switched on or off) to the master processor of the data acquisition system through the OS9 software pipe system [19]. The processor can be accessed remotely through the local area network.

7.2 Powering system

The powering system of the μVTX2 had to be doubled for the μVTX3, and it was more cost effective to replace it with a complete newly designed system. The new powering system was developed and produced from a detailed OPAL specification by DPS S.A. [33]. It consists of six crates, each with ten identical power modules. Each power module provides the bias voltages for one ladder and the low voltages for amplifiers and electronics for a ladder pair. Every fourth module also provides the low voltage power for the ICR PCB electronics.

The power modules have regulators for each of their 12 power channels. The input power to the regulators is provided by power supplies that are in common to the entire crate. The ground of the crate is floating, but the grounds of the individual modules in a crate are connected via the regulators which create a high impedance path. The reference voltages for the regulators are supplied by a DAC.

Each crate also contains a controller module equipped with a standard microcontroller chip that interfaces to an RS422 serial interface and is able to set voltages (by setting the DAC of a power module) and to read voltages and currents (from a multiplexed ADC in each power module). In addition status information is available from the controller module. The controllers can be put in series following the RS422 protocol and each controller is identified by a unique address that is set by jumpers on the controller module. Special care is taken to ensure a fail-safe operation of the power supplies. Voltages can be switched on only when a current flows in a current loop. The power modules are also capable of breaking this current loop, for example if the module hardware or the main power were to fail.

The power supplies are connected to a RS422 interface Industrypack module [34], which is mounted on an Industrypack–VME interface board [35], and is controlled by the MVME167 CPU. The CPU issues commands and each command provokes a response from exactly one power supply controller.

Voltages are ramped by issuing a sequence of steps from the controlling microprocessor. After a number of steps the currents are checked by reading them out and comparing them to limits in the MVME167 CPU. After the voltages reach their set values, voltages and currents continue to be checked in the same way, reading them and comparing them to reference values in the MVME167 CPU.

7.3 Interlock system

At the end of the 1994 LEP run the μVTX2 accidentally overheated in an incident in which the cooling failed, but the detector remained powered. Although the system was in principle protected against this problem, an unexpected combination of events brought about this failure. After this incident many ladders were no longer operational and the detector was removed from OPAL before the end of the LEP run. In the winter shutdown of 1994–1995 all the damaged ladders were repaired to their original quality. The most common problem was broken bond wires between the pitch adapter and the first detector wafer. It was also found that the Woods metal used for soldering the cooling tube of the μVTX2 in the support ring had melted. An Indium alloy of higher melting point is now used for soldering this cooling tube in the μVTX3.

The other consequence of this incident was the commissioning of a new comprehensive interlock system to enhance the safety of operation of the μVTX3. This system consists of a current loop, as illustrated in Fig. 12. When the current loop is broken both the powering and cooling systems are switched off. The warm parts of the detector then cool to ambient temperature after about 10 to 15 minutes due to the cold reservoir formed by the cooling system

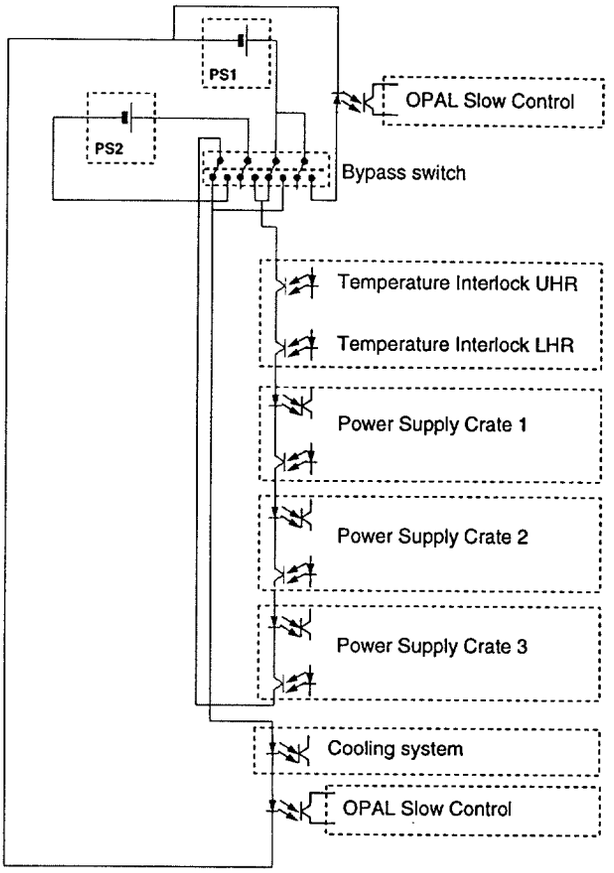

Figure 12: *Current loop interlock system for the μVTX3. The two temperature interlocks act based on one temperature sensor on the Upper Half Ring (UHR) and one sensor on the Lower Half Ring (LHR).*

and surrounding material, and the reservoir warms up slowly over a time scale of about one hour.

There are two main mechanisms that may break the current loop. The powering system will break the current loop if the main power fails, if one of the common low voltage power supplies of the crate runs out of specification, or if the EPROM software in one of the controller modules fails. The other main mechanism to break the current loop is through a dedicated module that compares voltages from several thermistors against their preset validity ranges that correspond to temperatures for safe detector operation. The current loop breaks if one of the thermistors indicates a temperature outside the valid range, or if there is a failure of the power to the module.

8 Software alignment procedure

A software alignment procedure is used to obtain optimum geometrical position reconstruction for detector hits. The method used for μVTX3 is similar to the procedure developed for μVTX2 [3]. The alignment is carried out in two stages. Initially, a set of global constants is determined, which corresponds to the overall movement of the detector array with respect to the other OPAL tracking components. Then a set of local constants, which allow for variations of the relative positions of the ladders and the detector wafers, is optimised.

The local constants are initially determined from the metrological survey prior to the insertion of the detector into OPAL (section 4). In contrast to the alignment procedure used for μVTX1 and μVTX2, the alignment of μVTX3 could not rely on di-lepton events since the number of these events available when LEP operates predominantly at centre-of-mass energies above the Z^0 resonance is insufficient. Hence multihadronic events had to be used exclusively for the optimisation of global and local alignment constants. Events to be used in the alignment procedure were required to have at least six tracks. Tracks inconsistent with a common vertex (e.g. due to heavy flavour decays) are removed iteratively until a satisfactory vertex is obtained. In an iterative procedure, the positions of the whole μVTX3 detector and of the ladders and wafers are modified to minimise the residuals of μVTX3 hits to considered tracks.

The ultimate position uncertainty resulting from the alignment is estimated to be about 8 to 10 μm in the r–ϕ and 10 to 12 μm in the r–z coordinates and is limited by the systematic errors of the overall OPAL tracking system.

9 Performance

9.1 1995 detector configuration

When installation took place for the 1995 LEP run, the full complement of short ladders was not yet available. It was decided to install the maximum number of ladders in a manageable configuration to gain experience in both installing and operating the new detector. Therefore the new detector support structure was installed. Sufficient short ladders were available to equip completely the outer layer. No short ladders were installed on the inner layer. The detector was positioned with the centre of the long ladders in the middle of OPAL. This configuration was then similar to the μVTX2 operation, but with the two additional long ladders added to complete the ϕ coverage, and the installation was virtually the same as for the fully equipped detector in 1996. During 1995 valuable experience was gained on the alignment of the overlapping and tilted ladder geometry and the relative alignment of the long and short ladders. The short ladders proved very stable in operation and the MX7-RH chips performed as expected, giving full confidence for the operation of the complete detector in the following years.

9.2 Operational experience

In 1996, the first year of full μVTX3 operation, the detector performed well. The new online pedestal and noise update scheme in the DSPs of the SIROCCOs, which ignores events with any track occupancy, has made the online pedestal and noise calculation in LEP2 operation as stable as for LEP1 running.

Some detector wafers are known to show increasing leakage currents with high humidity. The complete detector enclosure around the beam pipe is therefore sealed and flushed with dry nitrogen gas. Because of good sealing of this gas volume, the relative humidity has been maintained at less than a few percent.

Since 1994 the backplane bias voltage has been ramped down between physics runs, such that there was no potential across the silicon wafers. This has been very effective in avoiding any build-up of large ($\sim$1μA) leakage currents in the detector.

During LEP2 operation, the temperature swing of the beam pipe between the different running phases (idle, filling, ramping and colliding) is typically 2–3°C, much larger than was

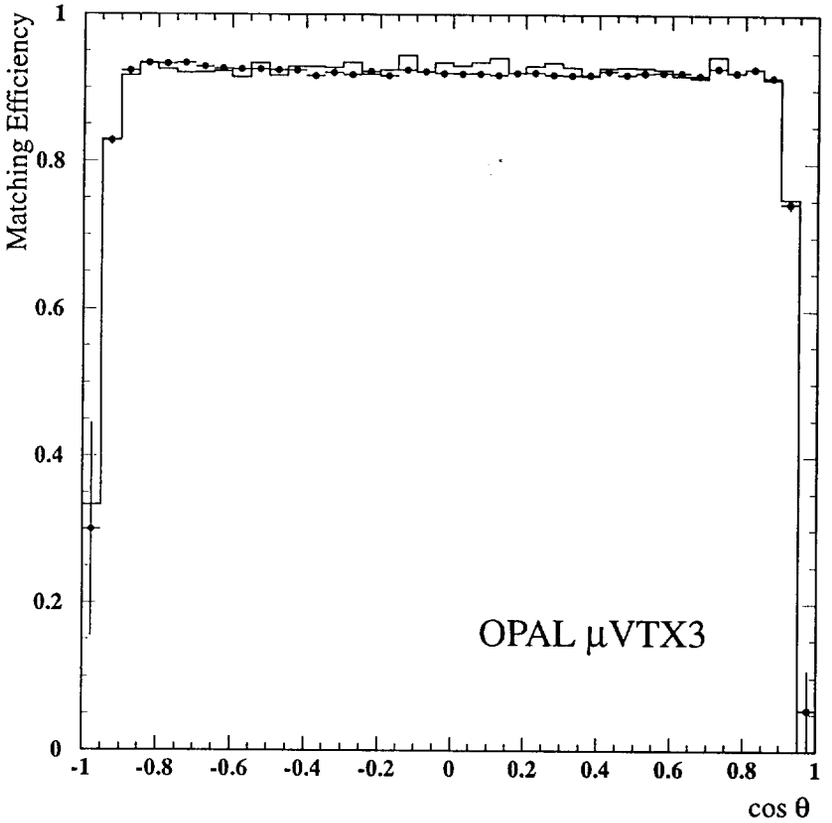

Figure 13: *Matching efficiency for two microvertex hits to central wire chamber tracks as a function of* $\cos\theta$ *for* $e^+e^- \to \mu^+\mu^-$ *events. The points with errors bars are the experimental data and the full line histogram is the Monte Carlo prediction.*

the case for LEP1. A temperature regulation program adjusts the amount of cooling depending on the temperature readings and keeps the temperature at the detector ladders stable to within 0.1°C (rms) with occasional short duration excursions up to 0.5°C, despite these beam pipe temperature variations. To date these temperature changes have had no noticeable effect on the detector performance or alignment.

The steady improvement of automatic monitoring and checking have significantly contributed to the successful operation of the OPAL microvertex detector.

9.3 Signal-to-noise ratio and detection efficiency

The peaks of the distributions of the signal-to-noise (S/N) ratios[‡] measured in the 1996 LEP run for all r–ϕ and z channels of the long and short ladders are shown in Fig. 14. For the short ladders the S/N values of 29:1 for r–ϕ and 25:1 for r–z for normal incidence correspond to total capacitive loading of the MX7-RH chips of 14 pF and 19 pF, respectively. The S/N values for normal incidence for the r–ϕ and z faces of the long ladders are 24:1 and 20:1. Given that the noise performance of their non-radiation hard MX7 chips is 350 + 15/pF (rms) electrons [3], the corresponding capacitive loads are 26 pF and 40 pF. The higher capacitance of the z-faces of the ladders result from the bussing lines of the z-prints.

[‡]The convention for S/N is that the signal is the sum of all channels in the cluster, while the noise is the average single channel noise for the channels in the cluster.

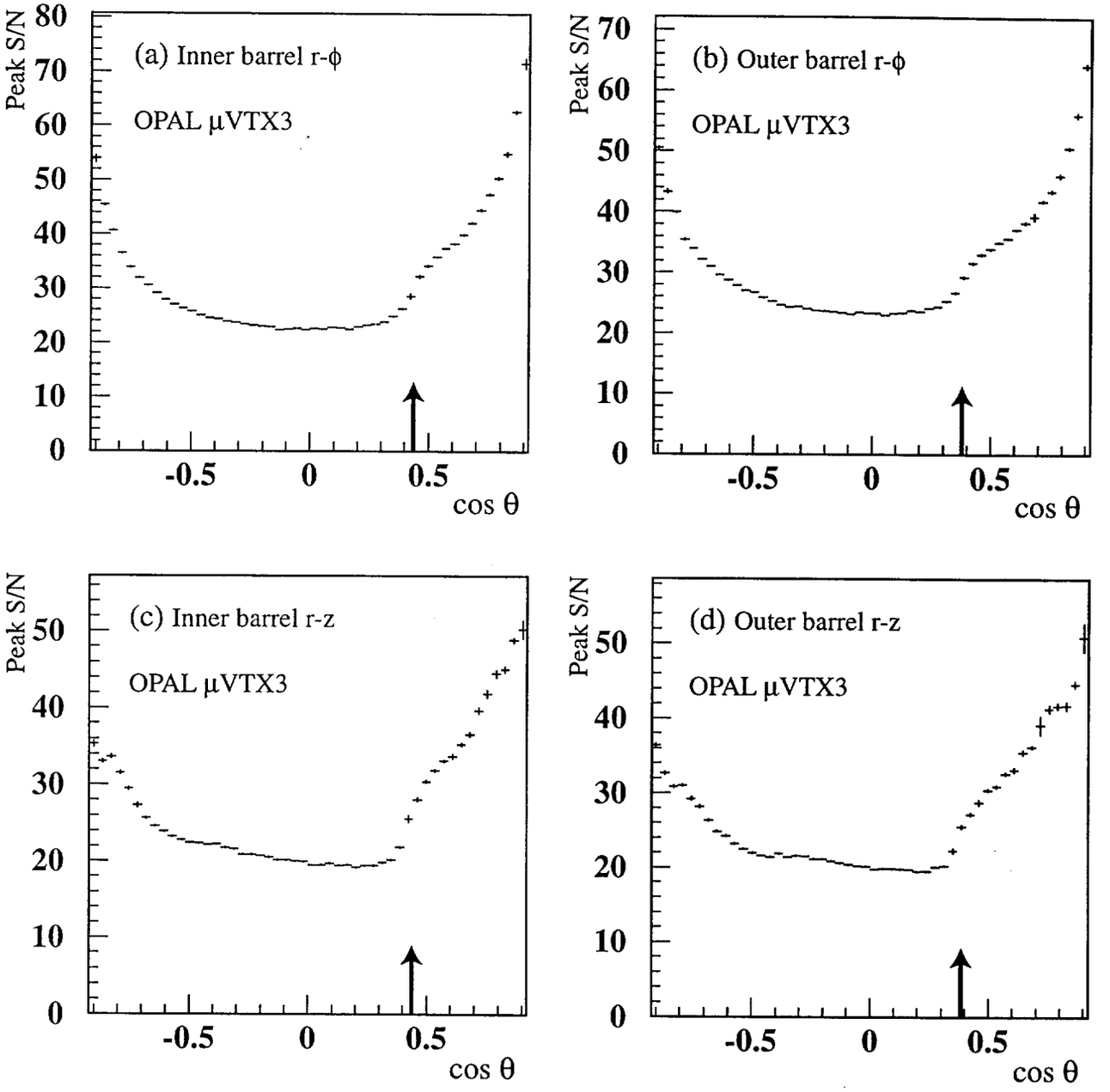

Figure 14: *Signal-to-noise (S/N) ratios for (a) all r–φ readout channels in the inner barrel, (b) all r–φ readout channels in the outer barrel, (c) all r–z readout channels in the inner barrel, and (d) all r–z readout channels in the outer barrel. The* $\cos\theta$ *value of the point where the long and short ladders join is indicated by the arrow.*

The overall efficiency for providing a microvertex hit matched to a reconstructed track in the wire chambers for minimum ionising particles traversing the active area of ladders is determined to be about 97% from di-lepton events. This is illustrated in Fig. 13, where the matching efficiency for two microvertex detector hits to central wire chamber tracks is shown to exhibit a value of 93% for nearly the entire $\cos\theta$ range. This number is the product of the silicon detector efficiency, the fraction of good working readout channels, and the online cluster finding efficiencies. The efficiency is the same for short and long ladders.

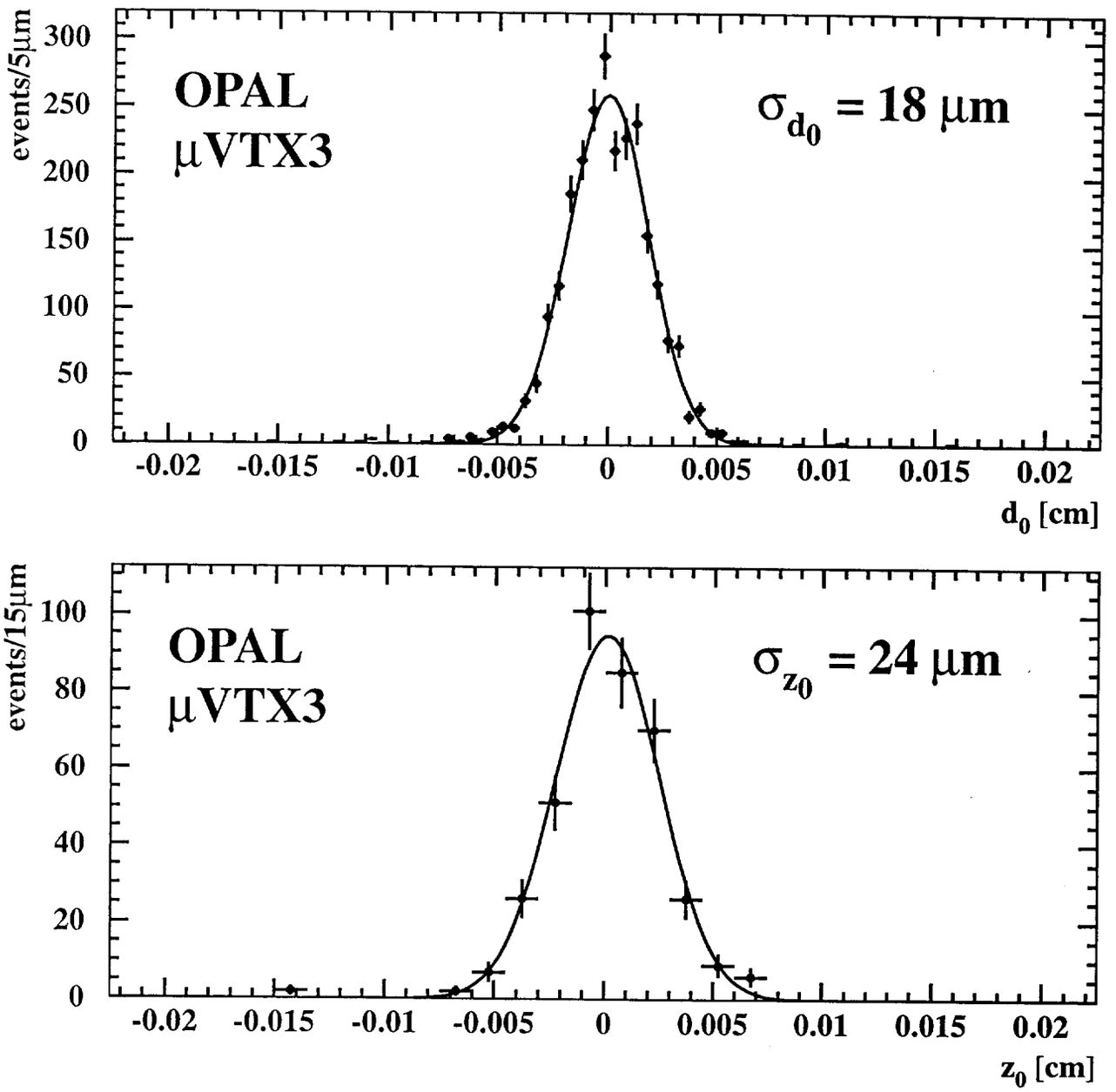

Figure 15: *Impact parameter distributions in the plane perpendicular to the beam axis (d_0) and in the direction of the beam axis (z_0) for $e^+e^- \to \ell^+\ell^-$ (ℓ =e,μ) events taken in 1996. The points with error bars are the data and the full line is a Gaussian fit.*

9.4 Impact parameter resolutions

The impact parameter resolution at high momentum is determined from lepton pair events from Z^0 decays. The resolutions for tracks from lepton pair events are shown in Fig. 15. In the plane perpendicular to the beam axis a resolution of $\sigma(d_0) = 18$ μm is achieved for tracks with $|\cos\theta| < 0.75$. In the direction of the beam axis a resolution of $\sigma(z_0) = 24$ μm is obtained for tracks emerging in the region normal to the beam direction. These values are slightly worse than for the μVTX2 detector, due to the less accurate alignment caused by the lower charged track statistics at LEP2 compared to LEP1.

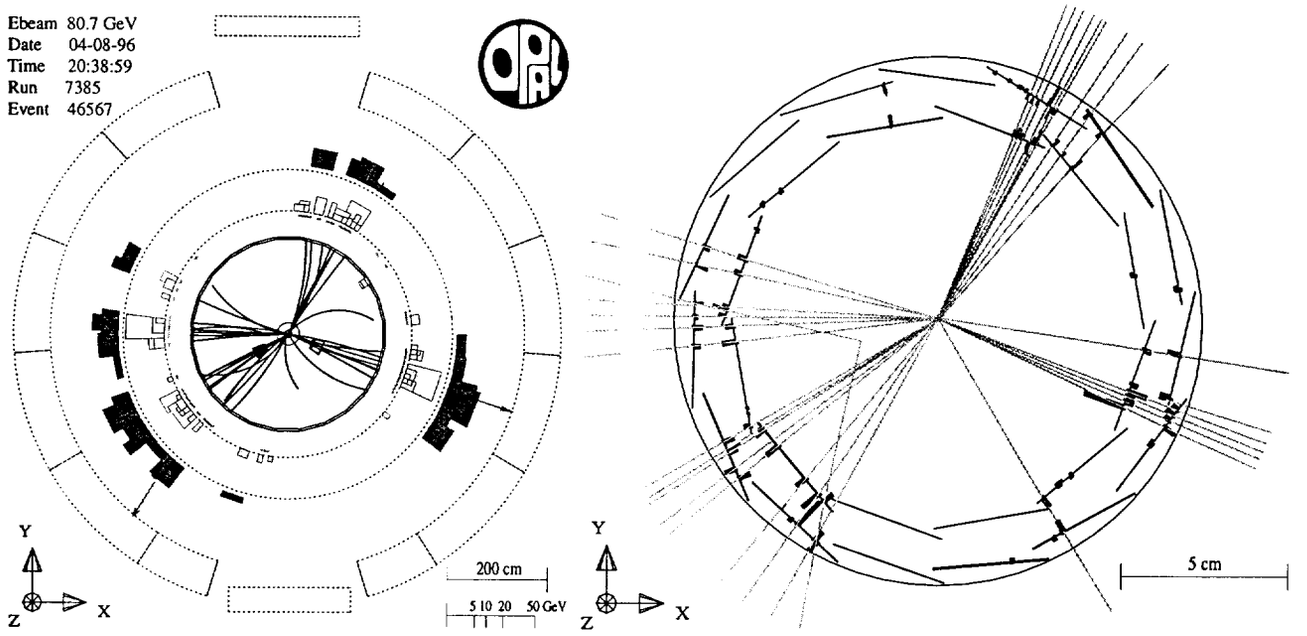

Figure 16: *Example of an $e^+e^- \rightarrow W^+W^-$ event at LEP2 as measured with the OPAL detector. The W bosons both decay into two jets. The left view shows the charged tracks and energy depositions reconstructed in the whole OPAL detector. The right view shows the hits in the microvertex detector, indicated by thick lines that start at the position of the hit and have a length proportional to the signal height.*

10 Conclusion

The extended OPAL silicon microvertex detector has been successfully constructed, installed and commissioned within the experiment. It performed very well during 1996, the first year of LEP2 data taking. An example of a typical LEP2 physics event, the production and hadronic decay of a pair of W particles ($e^+e^- \rightarrow W^+W^-$), is shown in Fig. 16, where it can be seen that nearly all reconstructed tracks have two matched microvertex detector hits. All but two tracks fit consistently with a single primary vertex. The remaining two tracks originate from a clearly visible neutral particle decay, showing the capability of reconstructing secondary vertices. In the upward direction two microvertex hits (one in each barrel) are seen that have no matching reconstructed track. Careful analysis of the event showed hits in the vertex chamber of OPAL for a low momentum track that was not reconstructed in the large volume OPAL jet chamber.

The geometrical coverage and efficiency of the detector are now such that it can also be used very effectively as a track veto or a photon conversion finder. For example, both these properties are used in analyses that search for final state events consisting of only photons.

Acknowledgements

We thank our colleagues in OPAL who helped in many aspects of this project, in particular T. Kawamoto from the University of Tokyo for his help in acquiring funding for SIROCCO modules, and J. Pinfold from the University of Alberta for his assistance with the powering system. We thank J. Zimmer from the Max Planck Institut für Kernphysik for his assistance in ladder assembly.
In addition to the support staff at our own institutions we are pleased to acknowledge the:
Department of Energy, USA,
Particle Physics and Astronomy Research Council, UK,
Natural Sciences and Engineering Research Council, Canada,
Israel Science Foundation, administered by the Israel Academy of Science and Humanities, Minerva Gesellschaft,
Japanese Ministry of Education, Science and Culture (the Monbusho) and a grant under the Monbusho International Science Research Program,
German Israeli Bi-national Science Foundation (GIF),
Bundesministerium für Forschung und Technologie, Germany,
National Research Council of Canada.

References

[1] OPAL Collab., K. Ahmet *et al.*, Nucl. Inst. and Meth. **A305** (1991) 275.

[2] P. P. Allport *et al.*, Nucl. Inst. and Meth. **A324** (1993) 34.

[3] P. P. Allport *et al.*, Nucl. Inst. and Meth. **A346** (1994) 476.

[4] OPAL Collab., G. Alexander *et al.*, Phys. Lett. **B374** (1996) 341.

[5] OPAL Collab., K. Ackerstaff *et al.*, Z. Phys. **C73** (1997) 397;
OPAL Collab., K. Akers *et al.*, Z. Phys. **C68** (1995) 531;
OPAL Collab., K. Akers *et al.*, Phys. Lett. **B350** (1995) 273;
OPAL Collab., K. Akers *et al.*, Z. Phys. **C67** (1995) 379.

[6] OPAL Collab., K. Ackerstaff *et al.*, Z. Phys. **C74** (1997) 1;
OPAL Collab., K. Akers *et al.*, Z. Phys. **C67** (1995) 365;
OPAL Collab., G. Alexander *et al.*, Phys. Lett. **B388** (1996) 659;
OPAL Collab., G. Alexander *et al.*, Z. Phys. **C69** (1996) 543;

[7] Physics at LEP2, Ed. G. Altarelli, T. Sjöstrand and F. Zwirner, CERN yellow report 96–01 (1996).

[8] O. Biebel et al., *The Radiation Monitoring and Beam Dump System of the OPAL Microvertex Detector*, CERN preprint CERN–PPE/97–091 (1997), Submitted to Nucl. Instr. Meth. **A**.

[9] Dexter, HYSOL EA9330 epoxy adhesive.

[10] The beryllium support half shells were produced by Brush Wellman, Theale, RGB 4BQ, UK.

[11] C1BA Araldite adhesive, AW106/HV953V.

[12] P. P. Allport et al., Nucl. Instr. Meth. **A310** (1991) 155.

[13] z-print processing by Optimask, Paris, France.

[14] E. Gross, *Routing of Z Readout Lines in the LEP Silicon Detectors*, In Proc. of the Third International Workshop on Vertex Detectors, Ed. R. Van Kooten, Lake Monroe, USA, Indiana University IUHEE-95-1, May 1995.

[15] WELL diamond wire saw, Walter Ebner S.A., CH-2400, Le Locle, Switzerland.

[16] Rotary ROD 456–4500, and linear LS406 scales by Heidenhain (Suisse) A.G., CH–8603 Schwerzenbach, Switzerland.

[17] Visulesta 10, Axesta A.G., CH–9008, St. Gallen, Switzerland.

[18] VME processor module MVME147 with MC68030 processor, by Motorola Inc., Phoenix, Arizona 85036, USA.

[19] OS9/68000 Operating System Technical Manual, Microware Systems Corp., Des Moines, Iowa 50322, USA, June 1987.

[20] FASTBUS version of the SIlicon Read Out Camac COntroller (SIROCCO), N. Bingefors and M. Burns, in M. Budinich et al. (eds.), Proc. Int. Conf. on the Impact of Digital Microelectronics and Microprocessors on Particle Physics, Trieste, Italy, 1988 (World Scientific, Singapore) p. 116.

[21] The design of the MX7 chip of reference [22] was changed to comply with the radiation hard process of Harris at the Rutherford Appleton Laboratory, UK. The chip was manufactured by Harris.

[22] The MX7 chip was designed at the Rutherford Appleton Laboratory, UK. The chip was manufactured by Mietec N.V., Oudenaarde, Belguim. The reference for microplex (MX) series chips is J. C. Stanton, IEEE Trans. Nucl. Sci. **36** (1989) 522.

[23] J. T. M. Baines et al., Nucl. Instr. Meth. **A325** (1993) 271.

[24] N. Arignon et al., Nucl. Instr. Meth. **A313** (1992) 103.

[25] FASTBUS-to-VSB Interface module FVSBI 9210 from CES, Petit-Lancy, Switzerland.

[26] FASTBUS communications processor used was a CES FIC8230 with MC68020 processor by CES, Petit-Lancy, Switzerland.

[27] VME processor module MVME167 with MC68040 processor, by Motorola Inc., Phoenix, Arizona 85036, USA.

[28] Digital Signal Processors used were Motorola DSP 56001, by Motorola Inc., Phoenix, Arizona 85036, USA.

[29] R. Hammarström, VME ADC module, Internal Note, Sept. 1988.

[30] VESTALE V15R, 1500 W and 1000 W battery backed up power supplies from Serras, Rungis, France.

[31] A. K. Amundsen et al., Nucl. Instr. and Meth. **A293** (1990) 145.

[32] P. C. Burkimsher, The EMU User Guide, CERN/CN Division.

[33] Power Supplies manufactured by DPS S.A., Rue du Pre-de-la-Fontaine 15, 1217 Meyrin, Switzerland.

[34] Industry Pack RS422 interface module from Tews Datentechnic GmbH, Am Bahnhof 7, D–25469 Halstenbek, Germany.

[35] VME Industry Pack carrier module from Greenspring Computers, O'Brien Drive 1204, CA–94025 Menlo Park, USA.